journal of the mechanical behavior of biomedical materials 128 (2022) 105078

Contents lists available at ScienceDirect

Journal of the Mechanical Behavior of Biomedical Materials

journal homepage: www.elsevier.com/locate/jmbbm

Sintering distortion of monolithic zirconia in 4-unit fixed partial denture: Effect of layered structure and vertical milling area

Mizuho Hirano *, Syuntaro Nomoto, Toru Sato, Mamoru Yotsuya, Ryuichi Hisanaga, Hideshi Sekine

Tokyo Dental College Dept. of Fixed Prosthodontics, Japan

ARTICLE INFO

Keywords:
Multi color layered zirconia
Yttria-partially stabilized zirconia (Y-PSZ)
Sintering distortion
Monolithic zirconia FPDs
All-ceramic crown
Dental ceramics

ABSTRACT

Layered-type zirconia disks, which offer color gradation from enamel to cervical shade, have been employed in recent years to replicate the shades of natural teeth. The layered structure is effective at replicating colors and has helped popularize monolithic zirconia restorations. However, the sintering shrinkage of zirconia is very large; thus, controlling the sintering distortion is very important. Thus, the objective of this study was to determine the influence exerted by the layered structure of the zirconia disk and the vertical milling area on the sintering distortion. An experimental fixed partial denture (FPD) was designed based on a 4-unit monolithic zirconia FPD. A single-composition (SC)-type disk with no shade and a single-composition-layered (SCL)-type disk with shade gradation were selected for this study. In particular, three milling areas, the top end of the disk (area I), vertical center (area II), and bottom end of the disk (area III), were investigated. Moreover, the sintering distortions generated by the experimental FPDs were measured. Results showed that sintering distortion in 4-unit monolithic zirconia FPDs occurred in all SC and SCL areas. Additionally, the sintering distortions were affected by the layered structure of the zirconia disks, the degree of which depended on the milling area (area I > area II > area III). Thus, when fabricating dental prosthesis using SCL zirconia disks, the milling area must be selected considering both the color adjustment and sintering distortion.

1. Introduction

Fixed partial dentures (FPDs) have been used in the field of prosthodontics for numerous years. They consist of retainers, which is fitted to the adjacent teeth, and a pontic, which replaces the missing tooth (Fig. 1). Traditionally, FPDs have been fabricated using precious and non-precious metals. However, the metallic color of FPDs does not appeal to the patients who require a natural tooth color for their prosthesis. Consequently, zirconia, with mechanical strength comparable to that of natural teeth, has been gaining interest. The excellent biocompatibility and mechanical characteristics of zirconia-based all-ceramic fixed partial dentures (FPDs) have been sufficiently verified (Harianawala et al., 2016; Ling et al., 2021; Maniconel et al., 2007). Moreover, their range of applications has been expanding and the current increase in the prices of noble metals has further accelerated this expansion.

Conventional zirconia is unnaturally white, significantly different from natural teeth with respect to color and translucency; thus, its esthetics limit its use as a single material in crown restorations. These concerns were addressed by veneering the outer surface of the zirconia framework with feldspar-based ceramics, which is similar in appearance to natural teeth (Baldissara et al., 2010; Guazzato et al., 2005). However, cases of delaminating and chipping affecting the veneering porcelain have been reported for the molar area owing to the restrictions it poses on abutment cutting and high masticatory force (Rinke et al., 2013; Sailer et al., 2006, 2007). Furthermore, there is a possibility that the accumulation of internal stress in the veneering porcelain firing cycles influences the marginal fit of the zirconia framework (Dittmer et al., 2009). Further, veneering porcelain requires the expertise of dental technicians (Stawarczyk et al., 2011), as well as a specified amount of time. Consequently, monolithic zirconia restorations, which have a low risk of fracture, have attracted significant attention as a solution to the above-mentioned issues (Öztürk and Can, 2019; Zhang et al., 2013). Monolithic zirconia restorations are fixed prosthesis entirely using zirconia without veneering (Fig. 2). This avoids the risk of veneer fracture. Moreover, to color-match white zirconia to the shade of natural teeth, colored zirconia was developed by adding metal oxide

* Corresponding author.
E-mail address: mhirano@tdc.ac.jp (M. Hirano).

https://doi.org/10.1016/j.jmbbm.2022.105078
Received 20 October 2021; Received in revised form 2 January 2022; Accepted 7 January 2022
Available online 19 January 2022

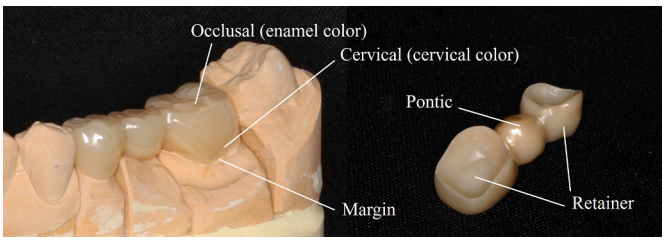

Fig. 1. Fixed partial denture
FPDs consist of retainers, which is placed on the adjacent tooth (abutment tooth), and a pontic, which fills the missing tooth. As a fixed prosthesis, it is used in the partially edentulous arch.

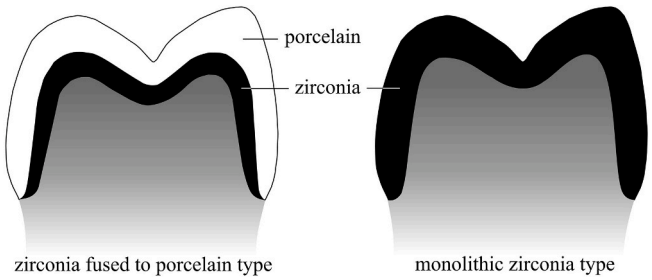

Fig. 2. Two types of zirconia all-ceramic crown
The zirconia fused to porcelain type has traditionally been used in prosthetic dentistry. The outer surface of the zirconia frame is coated by porcelain (e.g., feldspar ceramics) to achieve favorable aesthetics. Conversely, owing to the improved aesthetics combined with monolithic zirconia type, crown prostheses using only zirconia can be developed.

(Fe_2O_3) to adjust to the zirconia powder before molding, from which single-composition-layered (SCL)-type zirconia disks were developed (Fig. 3). These SCL-type zirconia disks which were developed to mimic the color gradations of natural teeth, were formed using color gradations over several layers from the enamel layer with a little metal oxide to the cervical layer that contains a high metal oxide content (Kolakarnprasert et al., 2019; Zhao et al., 2013). However, the layer composition ratios vary according to the manufacturer.

Furthermore, zirconia disks that are compatible with the commonly used VITAPAN classical shade have been commercialized and have become valuable in esthetic dental prosthesis. The layered-type zirconia disk offers the advantage of allowing fine adjustments to the shade by changing the vertical area (position relative to disk thickness) to be milled.

However, zirconia experiences approximately 20-25% linear shrinkage during the sintering process (Carter et al., 2009; Denry and Kelly, 2008; Heydecke et al., 2007; Renold and Ramesh, 2016). Therefore, shrinkage rates must be predicted and calculated before milling, because predicting the sintering shrinkage and controlling the sintering distortion are important factors to achieve an accurate fit of prosthetic crowns (Sachs et al., 2014). Moreover, a poor fit of the margin area is associated with a reduced fracture resistance of the prosthetic crown (Schriwer et al., 2017). Consequently, numerous studies have been conducted on the sintering shrinkage and fit of zirconia prosthetic restorations (Edwards et al., 2017; Kunii et al., 2007; Sachs et al., 2014). A good fit has been demonstrated to be achieved for long span FPDs as well as crowns (Sachs et al., 2014). However, none have reported on the relationship between disk selection and different areas of milling with the post-sintering distortion generated when manufacturing molar FPDs using pre-sintered SCL-type disks with color gradation. The milling area is determined primarily by shade expression; thus, a comparative study was conducted to investigate the effects exerted by the layered structure and vertical milling area of the zirconia disk on the sintering distortion.

The null hypotheses of this study were as follows: (1) Single-composition (SC) zirconia disks and SCL zirconia disks do not exhibit distortion during the post-sintering process; (2) the layered structure of zirconia disks does not affect the sintering distortion; and (3) the difference in the vertical milling area does not cause a change in sintering distortion.

2. Materials and methods

2.1. Experimental FPD design and data development

A stainless-steel experimental abutment tooth model (Tokyo Giken, Tokyo, Japan) with missing mandibular first molar and mandibular second premolar and mandibular second molar and mandibular first premolar assumed to be abutment teeth was manufactured. The design schematic and appearance are shown in Figs. 4-1 and Figs. 4-2, respectively. The diameters of the abutment teeth were 11 and 7 mm for the mandibular second molar and mandibular first premolar, respectively, while the vertical length was 5 mm. The abutment teeth were designed based on the assumption that the retainer was an all-ceramic crown. Further, the taper of the shaft surface was set to 6°. In addition, the margin was in the form of a deep chamfer, and the radius of curvature was set to 1 mm.

The abutment tooth model was manufactured assuming that the mandibular first molar and mandibular second premolar were missing. The mandibular second molar and mandibular first premolar were assumed to be the abutment teeth, and the retainer was a monolithic zirconia crown with a heavy chamfer margin.

An experimental FPD was designed employing a simplified shape of a 4-unit monolithic zirconia FPD (Figs. 5-1). The emergence profile was established with a 60° tilt from the crown margin to the outer 1 mm. The crown above this crown was cylindrical, without any contour. The occlusal surface thickness was 1.5 mm. The two retainers were

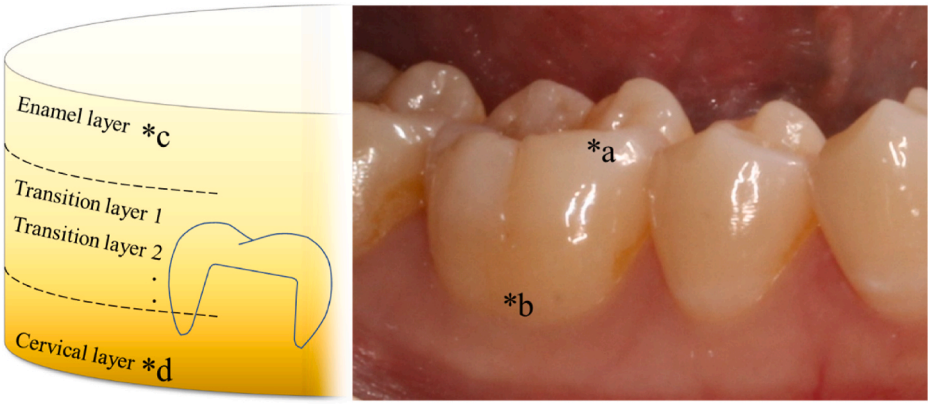

Fig. 3. Color gradation of SCL disks and natural teeth.
*a: The shade is lighter closer to the occlusal surface of the tooth.
*b: The shade is darker closer to the cervical of the tooth.
*c: The enamel layer is the light color part of the disk with a moderately low content of metal oxides.
*d: The cervical layer is the dark color part of the disk with a moderately high content of metal oxides.

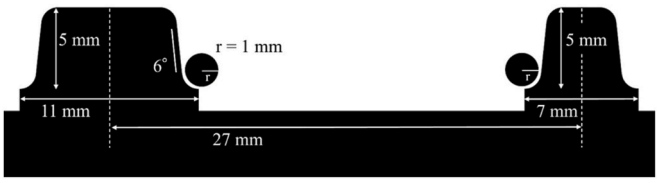

4-1 Schematic design of experimental abutment tooth model

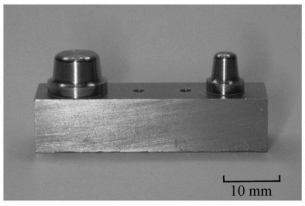

4-2 Appearance of experimental abutment tooth model

Fig. 4. Experimental abutment tooth model.

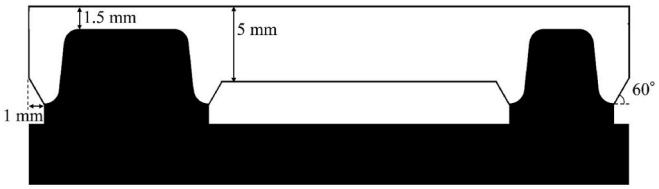

5-1 Schematic design of experimental FPDs

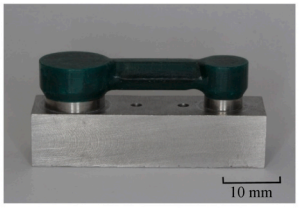

5-2 Wax pattern of experimental FPDs

Fig. 5. Experimental FPDs. Experimental FPDs assuming monolithic zirconia FPDs were waxed up.

connected via a hexagonal column with a cross-sectional area and vertical length of 22.5 mm^2 and 5 mm, respectively, which was used as the connector and pontic. Moreover, the retainers and pontics were linearly arranged.

A dental laboratory scanner (S-WAVE Scanner D2000, 3SHAPE, Copenhagen, Denmark) was used to scan the experimental abutment tooth model (Figs. 4-2) and the wax pattern (Figs. 5-2) to form the inner and outer surface of the experimental FPDs, respectively. Thereafter, the experimental FPDs were digitized and converted to standard triangulated language (STL) data by superimposing each of them with dental computer-aided-design (CAD) software (Dental Manager, 3Shape, Copenhagen, Denmark), and were subsequently used as the design data for FPDs (Fig. 6).

2.2. Experimental FPD milling and scanning

2.2.1. Experimental FPD milling

The details of the zirconia disks used in this study are listed in Table 1. Three SC-type and SCL-type disks were selected from each manufacturer. Disks with no shade were selected for the SC, where those with shades equivalent to the VITAPAN classical shade A3 from VITA were selected for the SCL. The disks were selected based on the following conditions: (1) thickness of 18 mm, (2) bending strength of 800 MPa or greater, (3) SC and SCL of the same manufacturer with equal amounts of added yttria, and (4) SC and SCL of the same manufacturer under the same sintering conditions.

The STL data of the experimental FPDs were imported into the dental computer-aided-manufacturing (CAM) software (GO2dental, Shofu, Kyoto, Japan), and the processing conditions were set according to the manufacturer instructions. The vertical milling area settings for each disk are shown in Fig. 7. Area I was positioned above the disk (0.1 mm inside the surface), area II was located at the center of the disk, and area III was located below the disk (0.1 mm beneath the surface). Seven experimental FPDs were milled using a dental milling machine (DWX-51D, Roland DG, Shizuoka, Japan) from each area (Fig. 8). Further, seven experimental FPDs from the same area were milled using a single disk.

2.2.2. Scanning of milled experimental FPDs

The milled (pre-sintering) experimental FPDs were scanned using a dental laboratory scanner (S-WAVE Scanner D2000, 3Shape, Copenhagen, Denmark) and converted to STL data. This was denoted as the control group (c) (n = 7).

2.3. Post-sintering and scanning of experimental FPDs

2.3.1. Post-sintering

Post-sintering of the experimental FPDs was conducted using a zirconia furnace (Esthemat Sinta ll, Shofu, Kyoto, Japan) under the conditions specified by the manufacturer (Table 2). One group (n = 7) of the

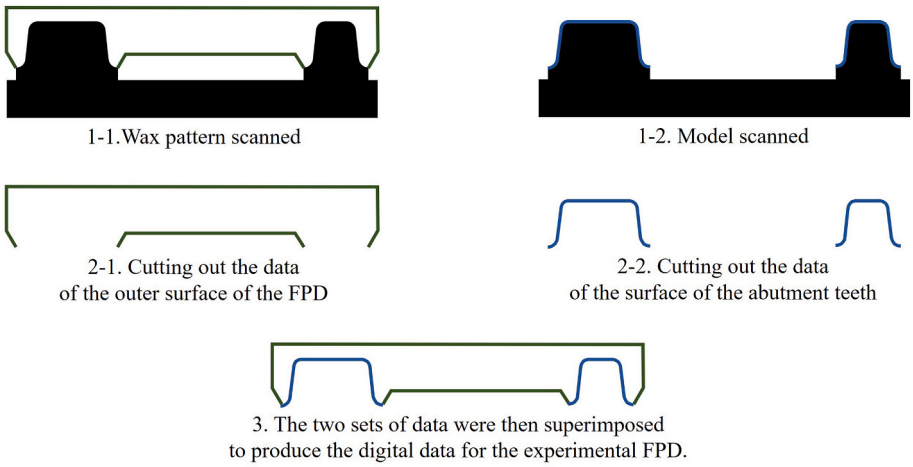

Fig. 6. Production of experimental FPDs data. Production of experimental FPDs data by superimposing two sets of data.

Table 1
Materials used.

Code	Product name	Shade	Yttria concentration (mol%)	Bending strength (MPa)	Manufacturer
SC-A	ZR lucent FA	Pearl white	5	1019	Shofu (A)
SCL-A	ZR lucent FA	5L medium			
SC-B	Katana (HT)	10C	4	1125	Kraray Noritake (B)
SCL-B	Katana (HTML)	A 3			
SC-C	DD Cube ONE	White	4	1250	Dental Direkt (C)
SCL-C	DD Cube ONE ML	A 3			

Single-composition-type (SC), single-composition-layered-type (SCL).

experimental FPDs was sintered in one cycle. The experimental FPDs were placed in a manner such that they did not touch each other. Subsequently, the sintered FPDs were ultrasonically cleaned in water for 5 min. Fig. 9 shows the post-sintering experimental FPDs.

2.3.2. *Scanning of post-sintering experimental FPDs*

The post-sintered experimental FPDs were scanned using a dental laboratory scanner (S-WAVE Scanner D2000, 3Shape, Copenhagen, Denmark), and the scans were converted to STL data. This was denoted as the experimental group (e) ($n = 7$).

2.4. *Measurement of pre- and post-sintering experimental FPDs*

The STL data of the control and experimental groups were imported into the CAD software (Fusion360(TM), AutoDesk Inc., San Rafael, USA). The buccolingual central cross section of the experimental FPDs was observed at a magnification of 910 times, and the margin measurement points included in the cross-section images (a–d) were marked (Figs. 10-1). Herein, a was connected to b, and c was connected to d using straight lines. Further, the external angle, α, formed by the two straight lines was measured using software. The intersection on the root side of the retainer margin was recorded as the case $\alpha > 0$ (Figs. 10-2), while the intersection on the crown side was recorded as $\alpha < 0$ (Figs. 10-3). Thus, the measured values were recorded for each experimental FPD.

The angle of the pre- and post-sintered experimental FPDs were α(c) and α(e), respectively, and the difference between them, α(e − c), was calculated. This was determined to be the sintering distortion caused by the post-sintering.

2.5. *Statistics*

First, the angle α(c) of pre-sintering and the corresponding angle α(e) of post-sintering in each group were compared using the Wilcoxon signed-rank test ($n = 7$). Thereafter, the sintering distortion α(e - c) corresponding to the SC and SCL of the same manufacturer were compared using the Wald–Wolfowitz runs test with three areas in each disk as a group ($n = 21$). Finally, the sintering distortions α(e - c) in areas I, II, and III of each disk were compared using the Kruskal–Wallis test and Dunn–Bonferroni multiple comparison tests ($n = 7$). The statistical software SPSS version 27 (IBM Corp., Armonk, NY, USA) was used, and the significance level was set at 1% and 5%.

3. Results

Table 3 and Table 4 shows the comparisons of average of the pre-sintering angle α(c) and post-sintering angle α(e) in each milling area of the disk. Significant differences were observed in the angles α(c) and α(e) for all areas of all disks.

Further, the sintering distortion α(e − c) of SC and SCL for each manufacturer was compared (Fig. 11). The vertical axes represent the sintering distortion α(e − c), whereas the horizontal axes represent the disk. A significant difference was observed between SC and SCL for all three manufacturers (A: $p = 0.001$, B: $p = 0.004$, C: $p = 0.001$); the sintering distortions α(e − c) of SC and SCL showed different distributions. Moreover, the SCL exhibited greater variability than the SC.

The sintering distortion α(e - c) in each area was compared for each disk (Fig. 12). A slight sintering distortion, indicated by a positive value of α(e - c), was observed in all SC types. However, these values were close to zero. In addition, no significant differences were observed between areas (SC-A, $p = 0.447$; SC-B, $p = 0.489$; SC-C, $p = 0.280$) (Fig. 12).

However, a more prominent difference in sintering distortion for each area was observed in SCL compared to SC (Fig. 12). The value increased in the ascending order of area I > area II > area III in all SCL types, with significant differences observed between areas I and III. Consequently, it was statistically determined that area I generated a larger sintering distortion. Furthermore, significant differences were observed in α(e - c) of areas I and II for SCL-A, and areas II and III for SCL-B and SCL-C (SCL-A, $p = 0.001$; SCL-B, $p = 0.001$; SCL-C, $p = 0.001$). Furthermore, a negative sintering distortion was observed in area III of SCL-B.

4. Discussion

4.1. *Shape of experimental FPDs*

The FPDs were manufactured to achieve a size as large as possible in this study to clearly observe sintering distortion. Thus, the 4-unit FPD, which is the largest FPD that can be supported by two abutment teeth in clinical applications, was used. Furthermore, the aim of this study was to analyze the influence of a layered structure on the sintering distortion of a prosthesis, and consequently, the sintering distortion caused by the shape of the prosthesis was eliminated to the maximum extent possible.

The complex shapes of zirconia prostheses produce distortions in the sintered body (Komine et al., 2005). However, to minimize any sintering distortion owing to the shape of the experimental FPD, the 4-unit FPD had a simplified shape. Kunii et al. (2007) demonstrated that sintering

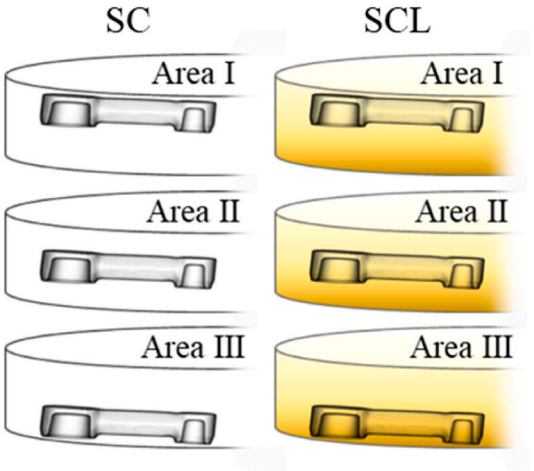

Fig. 7. Vertical milling area of experimental FPDs in the zirconia diskArea I was positioned above the disk, area II vertically at the center of the disk, and area III below the disk. Areas I and III were positioned 0.1 mm away from the top and bottom surfaces of the disk, respectively.

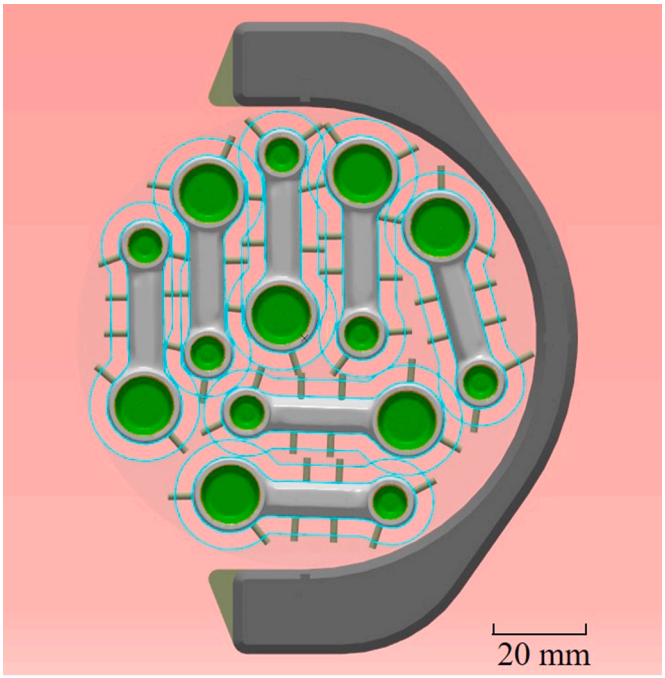

Fig. 8. Arrangement of experimental FPDs and support pins in disk
Seven experimental FPDs of the same group were placed in one disk (φ = 98). Support 2–3 pins were placed in the retainer and 4 in the pontic.

shrinkage of pontic influences the sintering distortion and that a poor fit has a higher risk of manifesting on the pontic side than on the non-pontic side. Thus, imbalances in the shape were reduced to the maximum extent possible. Moreover, to connect both retainers under the same conditions, the pontics of the two teeth were evenly designed. Furthermore, as a curvilinear design is considered conducive to the sintering distortion of prosthesis (Komine et al., 2005; Sachs et al., 2014), for the experimental FPDs in this study, the retainers and pontics were designed in a straight line.

4.2. Disk selection

This study used the VITA classical shade A3, which is often used in clinical settings in Japan, and disks with a corresponding color shade. Furthermore, all selected disks met the condition of having a three-point bending strength greater or equal to 800 MPa, based on the ISO standard after referring to the published bending strength figures by the manufacturer (International Organization for Standardization, 2015). The selected disks had a thickness of 18 mm, which can be considered the average thickness of the disks manufactured by different manufacturers. Consequently, the SC and SCL disks from each manufacturer, having the same yttria content, and the same recommended sintering temperature were selected. The doping of zirconia with metal oxides has been reported to increase the bending strength (Obolkina et al., 2020). However, there is no effect on the mechanical strength when small amounts are doped, as in the case of dental zirconia (Alves et al., 2021). Therefore, the mechanical strengths of the SC and SCL disks to be compared were equal.

4.3. Configuration of milling areas

The milling area in the zirconia disk is selected by the dentist or dental technician. Horizontal and vertical milling areas are selected and determined in three dimensions. According to a report summarizing the properties of dental zirconia, the cold isostatic pressing method, the most common method for compacting ceramic powders, applies a uniform pressure to the zirconia powder (Kontonasaki et al., 2020). Furthermore, a study comparing the effect of processing conditions on the retentive force of a cone crown telescope reported that the horizontal milling area of the disk had no effect on the retention (Nakagawa et al., 2017). Therefore, it was inferred that the mechanical properties within the dental zirconia disks were uniform, and the horizontal milling area of the disk did not affect the sintering distortion. In this study, to investigate the effect of vertical milling area (I, II, III) on sintering distortion, an area was milled from one disk and every condition except for vertical milling area were set equally in each group.

After milling, the experimental FPD height was approximately 8.3 mm, using approximately 46% of the 18 mm-thick disks. The number and distribution ratios of the layers in the disks varied between manufacturers; however, the details of the layered structure were not disclosed by the manufacturers. The layer distribution ratio for SCL-B, which has four layers and color gradation, has been published, and a study was conducted based on that data (Ueda et al., 2015). Considering the setting conditions in this study based on this report, the experimental FPD contains all the layers in the disk when placed in area II in SCL-B. In addition, it can be inferred that certain layers are not included in the

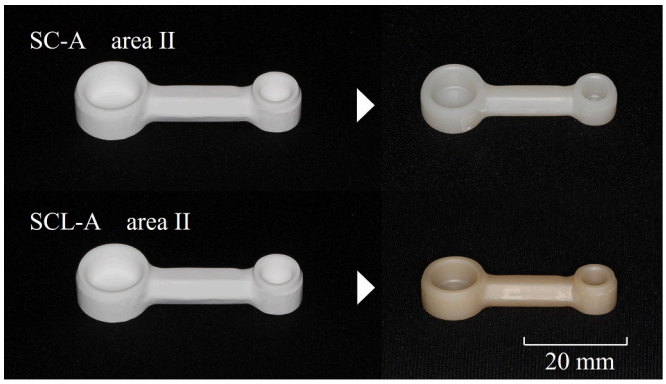

Fig. 9. Pre- and post-sintering experimental FPDs
The experimental FPDs were ultrasonically cleaned after post-sintering.

Table 2
Sintering program.

Code	Manufacturer	Sintering conditions				
		Heating rate	→	Plateau temperature and time	→	Cooling rate
SC-A SCL-A	Shofu (A)	5 °C/min	→	1450 °C 120 min	→	−10 °C/min
SC-B SCL-B	Kraray Noritake (B)	10 °C/min	→	1500 °C 120 mins	→	−10 °C/min
SC-C SCL-C	Dental Direkt (C)	8 °C/min	→ →	900 °C 30 mins 1450 °C 120 mins	→ →	3 °C/min −10 °C/min

Each experimental FPD was sintered according to the program recommended by the manufacturer.
Two-stage sintering was recommended for SC-C and SCL-C.

10-1 Margin measurement points

The measurement points were on the mesiodistal margins of both retainers in the buccolingual central cross-section of the experimental FPDs. Two points were connected by a line to each retainer.

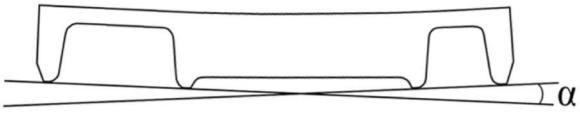

10-2 Measurement points when angle α > 0, that is, when the two lines intersect on the root side.

10-3 Measurement points when angle α < 0, that is, when the two lines intersect on the crown side.

Fig. 10. Margin measurement points and angle α measurement points.

layout when placed in areas I and III. Therefore, the number and ratio of layers included in the experimental FPDs, even those in the same area, would probably differ for each manufacturer. Further, the number of layers included in the experimental FPDs also changed, even if the same area was set, when disks with different thicknesses were selected. Thus, further investigations are needed to understand the manner in which these different settings affect the sintering distortion.

4.4. Sintering distortion of experimental zirconia FPDs

The first null hypothesis of this study is rejected, because the effect of the shape of the experimental FPD is involved. Further, the second null hypothesis is rejected. In addition, the third null hypothesis of this study is accepted for the SC and rejected for the SCL. Therefore, from these conclusions, in addition to the effect of shape, the layered structure of the metal oxide in SCL is considered to affect the sintering distortion.

4.4.1. Effect of FPD shape on sintering distortion

Microstructure observations of partially stabilized zirconia have shown that during post-sintering, the monoclinic phases disappear and transform to the tetragonal phase (Wertz et al., 2021). Here, a large shrinkage occurs (Scott, 1975). However, sintering distortion in prostheses is believed to be caused by insufficiently uniform sintering shrinkage (Edwards et al., 2017). According to Oh et al. (2010), who investigated the shrinkage rate of zirconia using a disk-shaped test piece, no significant differences were observed in the shrinkage rate of

Table 3
Comparison of pre-sintering and post-sintering angle α Comparison of pre-sintering and post-sintering angle α for each area on SC-type disk.

		angle α		Wilcoxon signed-rank test
		pre-sintered α(c)	post-sintered α(e)	
A	Area I	0.009086	0.108275	*
	Area II	0.009058	0.106938	*
	Area III	0.007489	0.090385	*
B	Area I	0.006912	0.140381	*
	Area II	0.008774	0.119450	*
	Area III	0.009651	0.129448	*
C	Area I	0.008489	0.132885	*
	Area II	0.009710	0.103999	*
	Area III	0.006198	0.113718	*

Table 4
Comparison of pre-sintering and post-sintering angle α. Comparison of pre-sintering and post-sintering angle α for each area on SCL-type disk.

		angle α		Wilcoxon signed-rank test
		pre-sintered α(c)	post-sintered α(e)	
A	Area I	0.008072	0.415242	*
	Area II	0.007097	0.238149	*
	Area III	0.008353	0.145195	*
B	Area I	0.009074	0.340804	*
	Area II	0.009956	0.226934	*
	Area III	0.008920	−0.259351	*
C	Area I	0.009661	0.465333	*
	Area II	0.009613	0.407837	*
	Area III	0.008101	0.215012	*

The pre-sintering angles α(c) and post-sintering angle α(e) in each area were compared using the Wilcoxon signed-rank test.

commercially available SC-type disks between the upper, middle, and lower parts. However, a study wherein zirconia was milled into a crown designed exhibited differences in the shrinkage amount because the thickness and shape differed depending on the crown site, resulting in distortions of the prosthetic prosthesis (Ohkuma et al., 2019). It was proposed that the differences in the shrinkage amount between the occlusal surface and cervical sides during the post-sintering process caused the sintering distortion in the experimental FPDs in this study. Although the experimental FPDs were designed to eliminate the effects of their shape on the sintering distortion to the maximum possible, they had a minimal FPD shape, which differed on the occlusal surface and margin sides. Therefore, it is possible that this caused a difference in shrinkage and affected sintering distortion (Table 3).

4.4.2. *Effect of differences in metal oxide amount on distortion*

The sintering distortion of the SCL varied more than that of the SC (Fig. 11). Metal oxide effects, in addition to the previously mentioned factor of FPD shape, may be the possible causes for this. SCL disks are manufactured by adding metal oxide in layer form to obtain a color gradation of the crowns. In particular, Fe_2O_3 is extensively used as an additive to impart the color of dentin and provides a dark brown hue to zirconia in proportion with an increase in its concentration (Holz et al., 2018; Jiang et al., 2015; Mendes et al., 2017). The SCL-B used in this study is the world's first SCL-type disk, which has been used in numerous studies (Ueda et al., 2015). A report on the composition and properties of SCL-B states that no metal oxide was detected in the enamel layer but was detected in the dentin layer (Kolakarnprasert et al., 2019). Thus, the SCLs, by other manufacturers, used in this study show similar trends.

Sintering-associated shrinkage commonly starts at 900–1000 °C (Boaro et al., 2003; Denry and Kelly, 2008; Kao et al., 2018) and stops at approximately 1500 °C. However, this is affected by the type and amount of additive used (Obolkina et al., 2020; Silva et al., 2014; Zhao et al., 2013). Adding metal oxide to zirconia is believed to accelerate the shrinkage speed and lower the temperature at which shrinkage starts. Kao et al. (2018) reported this temperature, 975 °C, for zirconia without added metal oxide, decreased to 925 and 900 °C when 0.25 and 1 mol % metal oxide, respectively, were added. As a result, sintering behaviors may vary between layers and exhibit slight differences in shrinkage starting temperatures in SCL disks, which are composed of layers with varying metal oxide concentrations. However, the sintering temperature of pre-sintered dental zirconia bodies is usually approximately 1000–1100 °C (Amat et al., 2020; Qian et al., 2016). Thus, it is inferred that the degree of shrinkage progression associated with pre-sintering for SCL disks varies depending on the layer. Moreover, it is also inferred that in the layer with advanced shrinkage in the pre-sintered state, the rate of shrinkage in the post-sintering process is lower than that in the layers where pre-sintered shrinkage is slow, and it is estimated that shrinkage during post-sintering is higher on the occlusal surface side than on the marginal side. This is consistent with the conclusions drawn by Suzuki et al. (2020) that the shrinkage rate and timing of each layer during post-sintering generated distortion differ between the layers.

Differences were observed in the sintering distortion between different areas in the SCL disks in the following order: area I > area II > area III (Fig. 12). Layers with a smaller added amount of metal oxide exhibit a larger rate of decrease in the shrinkage starting temperature (Kao et al., 2018). Furthermore, it has also been reported that the optimal amount of added metal oxide for expressing crown color was less than 0.1 mol (Willems et al., 2019). Therefore, it is likely that the sintering distortion increases as the area approaches closer to the enamel layer in the disk. Thus, this may be the cause of the higher sintering distortion in SCL area I than in area III as observed in this study.

Area III showed the least sintering distortion for SCL-A and SCL-C. However, distortion in the opposite direction from the others was observed in SCL-B-area III. The shade of this disk was the VITA classical shade A3, but the color differences and subtle shade changes in the disk were independently set by the manufacturer. Therefore, comparing the added amount of metal oxides with other disks whose shade is A3 is challenging, and it is not possible to unilaterally determine areas with little sintering distortion. In the future, it will be necessary to study the sintering distortion based on the composition and structure of the disk.

In addition, this information was obtained from simple experimental FPDs whose designs were not representative of actual crowns. Experiments with simple models have limitations in understanding the dimensional changes that occur in the complex structure of zirconia in

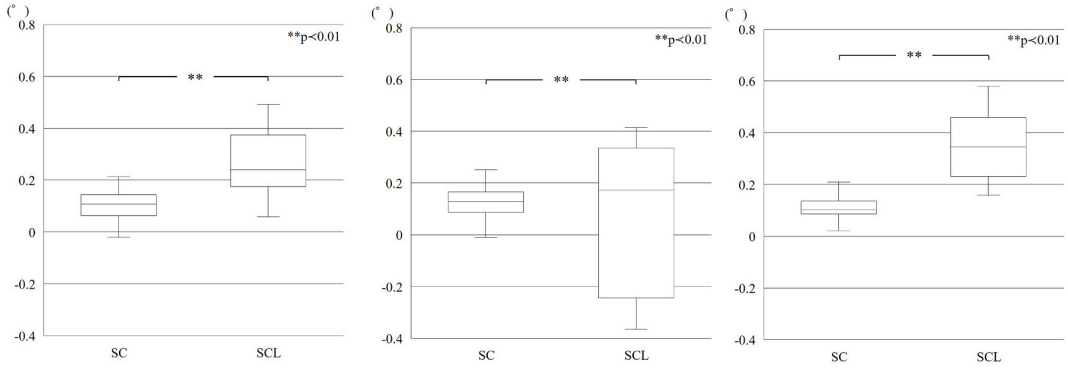

Fig. 11. Comparison of sintering distortion α(e − c) on SC and SCL-type disk
The sintering distortion α(e − c) in both disk types was compared using the Wald–Wolfowitz runs tests.

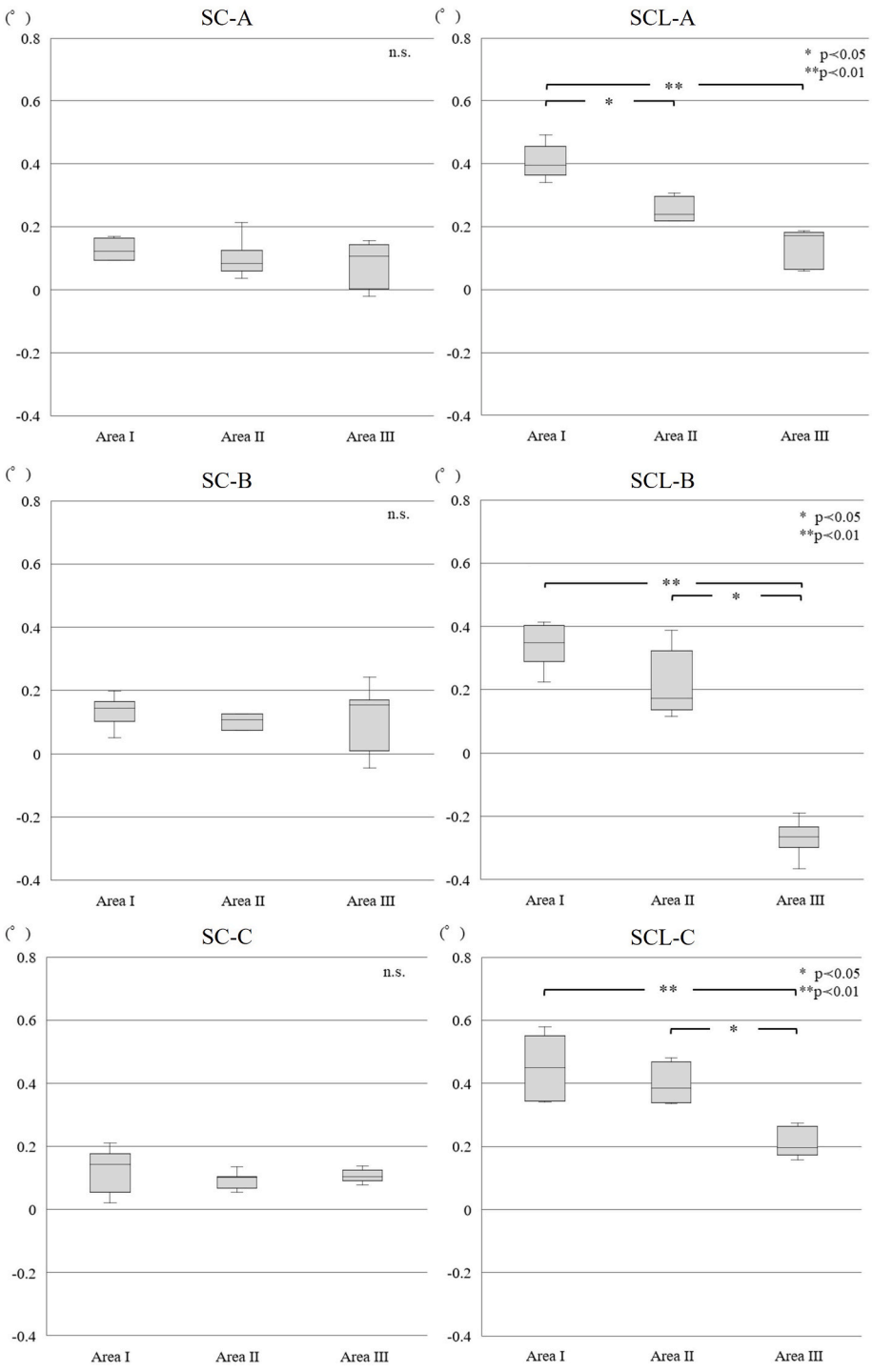

Fig. 12. Comparison of sintering distortion α(e − c) for each area
The horizontal axes represent areas, and the vertical axes represent the sintering distortion α(e − c).
The sintering distortion α(e − c) in each area was compared using the Kruskal–Wallis and Dann–Bonferroni tests.

prosthetic protheses (Ahmed et al., 2019). Thus, this is also a limitation of this study. Therefore, further studies are needed to better capture clinical conditions.

5. Conclusion

Based on the results obtained under the restrictions configured in this study, the following conclusions were drawn. Sintering distortions occurred in 4-unit monolithic zirconia FPDs. In particular, the layered structure of the metal oxide doped into the zirconia disks affected the sintering distortion. Large sintering distortions, the degree of which depended on the milling area, were observed in Area I. Therefore, when fabricating dental prosthesis with SCL zirconia disks, it is necessary to select the milling area considering not only the color adjustment but also the sintering distortion.

CRediT authorship contribution statement

Mizuho Hirano: Writing – original draft, Visualization, Methodology, Investigation, Formal analysis, Data curation. **Syuntaro Nomoto:**

Writing – original draft, Supervision, Methodology, Investigation. **Toru Sato:** Conceptualization. **Mamoru Yotsuya:** Writing – review & editing, Supervision. **Ryuichi Hisanaga:** Supervision. **Hideshi Sekine:** Writing – review & editing, Supervision, Resources, Project administration.

Declaration of competing interest

The authors declare that they have no known competing financial interests or personal relationships that could have appeared to influence the work reported in this paper.

Acknowledgements

The authors would like to thank Mr. Hirabayashi for the technical assistance with the experiments. We are also grateful to the reviewers for their comments. Finally, we would like to thank Editage (www.editage.com) for English language editing.

References

Ahmed, W.M., Abdallah, M.N., McCullagh, A.P., Wyatt, C.C.L., Troczynski, T., Carvalho, R.M., 2019. Marginal discrepancies of monolithic zirconia crowns: the influence of preparation designs and sintering techniques. J. Prosthodont. 28, 288–298. https://doi.org/10.1111/jopr.13021.

Alves, M.F.R.P., Ribeiroa, S., Suzuki, P.A., Strecker, K., dos Santosc, C., 2021. Effect of Fe_2O_3 addition and sintering temperature on mechanical properties and translucence of zirconia dental ceramics with different Y_2O_3 content. Mater. Res. 24 https://doi.org/10.1590/1980-5373-MR-2020-0402.

Amat, N.F., Muchtar, A., Yew, H.Z., Amril, M.S., Muhamud, R.L., 2020. Machinability of a newly developed pre-sintered zirconia block for dental crown applications. Mater. Lett. 261, 126996. https://doi.org/10.1016/j.matlet.2019.126996.

Baldissara, P., Llukacej, A., Ciocca, L., Valandro, F.L., Scotti, R., 2010. Translucency of zirconia copings made with different CAD/CAM systems School of Dentistry. J. Prosthet. Dent 104, 6–12. https://doi.org/10.1016/S0022-3913(10)60086-8.

Boaro, M., Vohs, J.M., Gorte, R.J., 2003. Synthesis of highly porous yttria-stabilized zirconia by tape-casting methods. J. Am. Ceram. Soc. 86, 395–400. https://doi.org/10.1111/j.1151-2916.2003.tb03311.x.

Carter, G.A., Hart, R.D., Rowles, M., Ogden, M.I., Buckley, C.E., 2009. Industrial precipitation of yttrium chloride and zirconyl chloride: effect of pH on ceramic properties for yttria partially stabilised zirconia. J. Alloys Compd. 480, 639–644. https://doi.org/10.1016/j.jallcom.2009.02.005.

Denry, I., Kelly, J.R., 2008. State of the art of zirconia for dental applications. Dent. Mater. 24, 299–307. https://doi.org/10.1016/j.dental.2007.05.007.

Dittmer, M.P., Borchers, L., Stiesch, M., Kohorst, P., 2009. Stresses and distortions within zirconia-fixed dental prostheses due to the veneering process. Acta Biomater. 5, 3231–3239. https://doi.org/10.1016/j.actbio.2009.04.025.

Edwards, R.C.E., Sanches, B.A.F., Macedo, R.M., Rubo, J.H., Griggs, J.A., 2017. Dimensional changes from the sintering process and fit of Y-TZP copings: micro-CT analysis. Dent. Mater. 33, e405–e413. https://doi.org/10.1016/j.dental.2017.08.191.

Guazzato, M., Quach, L., Albakry, M., Swain, M.V., 2005. Influence of surface and heat treatments on the flexural strength of Y-TZP dental ceramic. J. Dent. 33, 9–18. https://doi.org/10.1016/j.jdent.2004.07.001.

Harianawala, H., Kheur, M., Bal, A., Kheur, S., Sethi, T., Burhanpurwala, M., Sayed, F., 2016. Biocompatibility of zirconia. J. Adv. Med. Dent. Sci. Res. 4, 35–39.

Heydecke, G., Butz, F., Binder, J.R., Strub, J.R., 2007. Material characteristics of a novel shrinkage-free $ZrSiO_4$ ceramic for the fabrication of posterior crowns. Dent. Mater. 23, 785–791. https://doi.org/10.1016/j.dental.2006.06.015.

Holz, L., Macias, J., Vitorino, N., Fernandes, A.J.S., Costa, F.M., Almeida, M.M., 2018. Effect of Fe_2O_3 doping on colour and mechanical properties of Y-TZP ceramics. Ceram. Int. 44, 17962–17971. https://doi.org/10.1016/j.ceramint.2018.06.273.

International Organization for Standardization, 2015. Specifies the Requirements and the Corresponding Test Methods for Dental Ceramic Materials for Fixed All-Ceramic and Metal-Ceramic Restorations and Prostheses. ISO 6872:2015. https://www.iso.org/standard/59936.html.

Jiang, L., Wang, C.Y., Zheng, S.N., Xue, J., Zhou, J.L., Li, W., 2015. Effect of Fe_2O_3on optical properties of zirconia dental ceramic. Chin. J. Dent. Res. 18, 35–40.

Kao, C.T., Tuan, W.H., Liu, C.Y., Chen, S.C., 2018. Effect of iron oxide coloring agent on the sintering behavior of dental yttria-stabilized zirconia. Ceram. Int. 44, 4689–4693. https://doi.org/10.1016/j.ceramint.2017.12.049.

Kolakarnprasert, N., Kaizer, M.R., Kim, D.K., Zhang, Y., 2019. New multi-layered zirconias: composition, microstructure and translucency. Dent. Mater. 35, 797–806. https://doi.org/10.1016/j.dental.2019.02.017.

Komine, F., Gerds, T., Witkowski, S., Strub, J.R., 2005. Influence of framework configuration on the marginal adaptation of zirconium dioxide ceramic anterior four-unit frameworks. Acta Odontol. Scand. 63, 361–366. https://doi.org/10.1080/00016350500264313.

Kontonasaki, E., Giasimakopoulos, P., Rigos, A.E., 2020. Strength and aging resistance of monolithic zirconia: an update to current knowledge. Jpn. Dent. Sci. Rev. 56, 1–23. https://doi.org/10.1016/j.jdsr.2019.09.002.

Kunii, J., Hotta, Y., Tamaki, Y., Ozawa, A., Kobayashi, Y., Fujishima, A., Miyazaki, T., Fujiwara, T., 2007. Effect of sintering on the marginal and internal fit of CAD/CAM-fabricated zirconia frameworks. Dent. Mater. J. 26, 820–826. https://doi.org/10.4012/dmj.26.820.

Ling, Y., Li, Q., Zheng, H., Omran, M., Gao, L., Chen, J., Chen, G., 2021. Optimisation on the stability of CaO-doped partially stabilized zirconia by microwave heating. Ceram. Int. 47, 8067–8074. https://doi.org/10.1016/j.ceramint.2020.11.161.

Maniconel, P.F., Iommetti, P.R., Raffaelli, L., Paolantonio, M., Rossi, G., Berardi, D., Perfetti, G., 2007. Biological considerations on the use of zirconia for dental devices. Int. J. Immunopathol. Pharmacol. 20, 9–12. https://doi.org/10.1177/039463200702001s03.

Mendes, P.F.C., Elias, C.N., Santos, H.E.S., 2017. Effect of Fe_2O_3 addition in yttria-stabilized zirconia properties. Rev. Mater. 22 https://doi.org/10.1590/s1517-707620170002.0166.

Nakagawa, S., Torii, K., Tanaka, J., Tanaka, M., 2017. Retentive force of the cone crown telescope prosthesis using ceriastabilized- zirconia/alumina nanocomposite with a CAD/CAM system. J. Osaka Dent. Univ. 51, 55–62. https://doi.org/10.18905/jodu.51.1_55.

Obolkina, T.O., Goldberg, M.A., Smirnov, V.V., Smirnov, S.V., Titov, D.D., Konovalov, A. A., Kudryavtsev, E.A., Antonova, O.S., Barinov, S.M., Komlev, V.S., 2020. Increasing the sintering rate and strength of ZrO_2–Al_2O_3 ceramic materials by iron oxide additions. Inorg. Mater. 56, 182–189. https://doi.org/10.1134/S0020168520020156.

Oh, G.J., Yun, K.D., Lee, K.M., Lim, H.P., Park, S.W., 2010. Sintering behavior and mechanical properties of zirconia compacts fabricated by uniaxial press forming. J. Adv. Prosthodont. 2, 81–87. https://doi.org/10.4047/jap.2010.2.3.81.

Ohkuma, K., Kameda, T., Terada, K., 2019. Five-axis laser milling system that realizes more accurate zirconia CAD/CAM crowns by direct milling from fully sintered blocks. Dent. Mater. J. 38, 52–60. https://doi.org/10.4012/dmj.2017-443.

Öztürk, C., Can, G., 2019. Effect of sintering parameters on the mechanical properties of monolithic zirconia. J. Dent. Res. Dent. Clin. Dent. Prospects 13, 247–252. https://doi.org/10.15171/joddd.2019.038.

Qian, H., Cui, C., Su, T., Zhang, F., Sun, J., 2016. Exploring the optimal pre-sintering temperature on compressive strength and anti-fatigue property of graded zirconia-based glass/zirconia structure. Dent. Mater. J. 35, 341–344. https://doi.org/10.4012/dmj.2015-184.

Renold, E.S., Ramesh, T., 2016. Shrinkage characteristics studies on conventional sintered zirconia toughened alumina using computed tomography imaging technique. Int. J. Refract. Met. Hard Mater. 54, 383–394. https://doi.org/10.1016/j.ijrmhm.2015.09.008.

Rinke, S., Gersdorff, N., Lange, K., Roediger, M., 2013. Prospective evaluation of zirconia posterior fixed partial dentures: 7-year clinical results. Int. J. Prosthodont. (IJP) 26, 164–171. https://doi.org/10.11607/ijp.3229.

Sachs, C., Groesser, J., Stadelmann, M., Schweiger, J., Erdelt, K., Beuer, F., 2014. Full-arch prostheses from translucent zirconia: accuracy of fit. Dent. Mater. 30, 817–823. https://doi.org/10.1016/j.dental.2014.05.001.

Sailer, I., Fehér, A., Filser, F., Gauckler, L.J., Lüthy, H., Hämmerle, C.H.F., 2007. Five-year clinical results of zirconia frameworks for posterior fixed partial dentures. Int. J. Prosthodont. (IJP) 20, 383–388.

Sailer, I., Fehér, A., Filser, F., Lüthy, H., Gauckler, L.J., Schärer, P., Franz Hämmerle, C. H., 2006. Prospective clinical study of zirconia posterior fixed partial dentures: 3-year follow-up. Quintessence Int. 37, 685–693.

Schriwer, C., Skjold, A., Gjerdet, N.R., Øilo, M., 2017. Monolithic zirconia dental crowns. Internal fit, margin quality, fracture mode and load at fracture. Dent. Mater. 33, 1012–1020. https://doi.org/10.1016/j.dental.2017.06.009.

Scott, H.G., 1975. Phase relationships in the zirconia-yttria system. J. Mater. Sci. 10, 1527–1535. https://doi.org/10.1007/BF01031853.

Silva, P.C., Magnago, R.O., Silva, C.A.A., Fortes, B.A., Santos, C., 2014. Effect of particle size of $ZrO_2(Y_2O_3)$ powders on the shrinkage of the sintered substrate with coloring gradient. Adv. Sci. Technol. 87, 162–168.

Stawarczyk, B., Özcan, M., Roos, M., Trottmann, A., Sailer, I., Hämmerle, C.H.F., 2011. Load-bearing capacity and failure types of anterior zirconia crowns veneered with overpressing and layering techniques. Dent. Mater. 27, 1045–1053. https://doi.org/10.1016/j.dental.2011.07.006.

Suzuki, S., Katsuta, Y., Ueda, K., Watanabe, F., 2020. Marginal and internal fit of three-unit zirconia fixed dental prostheses: effects of prosthesis design, cement space, and zirconia type. J. Prosthodont. Res. 64 (4), 460–467. https://doi.org/10.1016/j.jpor.2019.12.005.

Ueda, K., Güth, J.F., Erdelt, K., Stimmelmayr, M., Kappert, H., Beuer, F., 2015. Light transmittance by a multi-coloured zirconia material. Dent. Mater. J. 34, 310–314. https://doi.org/10.4012/dmj.2014-238.

Wertz, M., Hoelzig, H., Kloess, G., Hahnel, S., Koenig, A., 2021. Influence of manufacturing regimes on the phase transformation of dental zirconia. Mater 14, 4980. https://doi.org/10.3390/MA14174980, 2021.

Willems, E., Zhang, F., Van Meerbeek, B., Vleugels, J., 2019. Iron oxide colouring of highly-translucent 3Y-TZP ceramics for dental restorations. J. Eur. Ceram. Soc. 39, 499–507. https://doi.org/10.1016/j.jeurceramsoc.2018.09.043.

Zhang, Y., Lee, J.J.W., Srikanth, R., Lawn, B.R., 2013. Edge chipping and flexural resistance of monolithic ceramics. Dent. Mater. 29, 1201–1208. https://doi.org/10.1016/j.dental.2013.09.004.

Zhao, J., Shen, Z., Si, W., Wang, X., 2013. Bi-colored zirconia as dental restoration ceramics. Ceram. Int. 39, 9277–9283. https://doi.org/10.1016/j.ceramint.2013.05.036.